ACS APPLIED MATERIALS & INTERFACES

Research Article

www.acsami.org

# $C_{60}/Bi_2TiO_4F_2$ Heterojunction Photocatalysts with Enhanced Visible-Light Activity for Environmental Remediation

Guisheng Li,* Bo Jiang, Xin Li, Zichao Lian, Shuning Xiao, Jian Zhu,* Dieqing Zhang, and Hexing Li

Department of Chemistry, Key Laboratory of Resource Chemistry of Ministry of Education, Shanghai Normal University, Shanghai 200234, China

Supporting Information

**ABSTRACT:** Fullerene ($C_{60}$)-enhanced $B_{i2}TiO_4F_2$ hierarchical microspheres were prepared by a facile solvothermal method. Compared to the pure $Bi_2TiO_4F_2$ photocatalyst, the $C_{60}/Bi_2TiO_4F_2$ samples exhibit much stronger photocatalytic performance for degrading Rhodamine B (RhB) and Eosin Y (EY) under visible light irradiation. Such greatly enhanced photocatalytic activity may be ascribed to strong combination and heterojunctions between $C_{60}$ and $Bi_2TiO_4F_2$, favorable for charge separation and light adsorption. Loading $C_{60}$ on $Bi_2TiO_4F_2$ results in a new photocatalytic mechanism (based on photo-generated $h_{vb}^+$ and $\cdot O_2^-$ radicals) different from that of pure $Bi_2TiO_4F_2$.

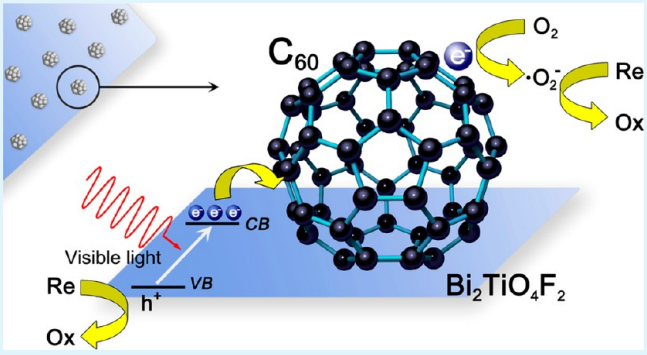


**KEYWORDS:** *$C_{60}$, $Bi_2TiO_4F_2$, heterojunctions, charge separation, photocatalytic*

## 1. INTRODUCTION

A large number of chemical pollutants such as synthetic textile dyes, and fluorescein dyes are harmful to the environment, hazardous to human health and normally difficult to be decomposed by natural means.[1] Lots of research on photocatalysis for environmental remediation has been mostly focused on $TiO_2$-based photocatalysts owing to their physical and chemical stability, low cost, availability, non-toxicity, and cheapness.[2] However, $TiO_2$ only actives in the UV range which merely occupies around 4 % of the received solar energy because of its wide band gap ($E_g \approx 3.2$ eV). Therefore, many studies have focused on the search for utilizing visible light for the treatment of pollutants by doping with hybrid atoms and coupling with other low band gaps semiconductors.[3,4]

Our earlier findings revealed that $Bi_2TiO_4F_2$ can serve as a new visible-light-driven photocatalyst for decomposing Dye wastewater with excellent stability.[5] Nevertheless, its photocatalytic performance is still limited owing to its poor electron-conducting capability and low quantum efficiency. Fortunately, $C_{60}$ was proved as a promoter for increasing the photoconversion efficiency of solar energy of solar cell via closely combining $C_{60}$ with semiconductor nanoparticles.[6,7] Thus, it is reasonable that the combination of $Bi_2TiO_4F_2$ and $C_{60}$ could also be an ideal route to achieving an enhanced charge separation efficiency for accelerating photo-induced electron transfer from $Bi_2TiO_4F_2$ to reaction system and improving the photocatalytic quantum efficiency of $Bi_2TiO_4F_2$. Such approach mainly relies on the efficacy on the excellent exciton mobility and relatively large exciton diffusion length ascribed to $C_{60}$ molecules.[8,9] As known, the delocalized conjugated structures of $C_{60}$ molecules allow the weak absorption in the visible range and the high electron mobility (> 1.3 $cm^2\ V^{-1}\ S^{-1}$).[10,11]

In the present work, $C_{60}/Bi_2TiO_4F_2$ hierarchical microspheres were prepared by a routine hydrothermal process. $C_{60}$ were highly dispersed on the surface of the $Bi_2TiO_4F_2$ crystals with a very close combination. Various organic pollutants (Rhodamine B, methyl orange, and Eosin Y) were utilized as target pollutants to examine the photocatalytic activity of the as-prepared $C_{60}/Bi_2TiO_4F_2$ composites under visible-light irradiation ($\lambda$ > 420 nm). The modification of $C_{60}$ greatly enhanced the photocatalytic performance of $Bi_2TiO_4F_2$ in oxidizing organic pollutants with an excellent stability. It was also found that the organic pollutants can be directly oxidized by both $h_{vb+}$ and ·OH radicals in the present $C_{60}/Bi_2TiO_4F_2$ photocatalytic system.

## 2. EXPERIMENTAL SECTION

All chemicals were analytical grade and used without further purification. Bismuth nitrate ($Bi(NO_3)_3{\cdot}5H_2O$) was provided by Sinopharm Chemical Reagent Co., Ltd. (Shanghai, China). Ethylene glycol (EG) and toluene were obtained from Shanghai Chemical Company. Titanium Tetrafluoride ($TiF_4$) and $C_{60}$ were obtained from Sigma-Aldrich Chemical Company. *Tert*-butyl alcohol (TBA) was obtained from Aladdin Chemical Company.

**Sample Preparation.** In a typical synthesis procedure, 0.08 g of $TiF_4$ was dissolved in 20 mL of *tert*-butyl alcohol (TBA) under ultrasonication at 25 °C with the formation of solution A; 6.24 g of $Bi(NO_3)_3{\cdot}5H_2O$ was dissolved in 5 mL of ethylene glycol (EG) via

Received: April 24, 2013
Accepted: July 8, 2013
Published: July 8, 2013

  

vigorous stirring at 25 °C with the formation of clear solution B. Then, solution B was added into solution A via vigorous stirring to form solution C. An appropriate amount of transparent $C_{60}$-toluene solution (1.0 g/L) with red color was added to solution C via vigorous stirring for 5 min and further transferred to an autoclave (50 mL) at 160 °C for 24 h. Subsequently, the autoclaved was cooled to room temperature naturally. The as-obtained gray samples were centrifuged, washed with deionized water and alcohol three times, and dried at 80 °C in a vacuum for 12 h for further utilization and characterization.

**Catalyst Characterization.** The crystal structures of the as-prepared samples were determined by X-ray diffraction (XRD, D/MAX-2000 with Cu Ka1 irradiation), scanning electron microscopy (SEM, JEOL JSM-6380LV) and transmission electronic micrograph (TEM, JEM-2010, operated at 200 kV), $N_2$ adsorption−desorption (Quantachrome NOVA 4000e, at 77 K). Light absorbance was measured by UV−visible diffuse reflectance spectroscopy (DRS, MC-2530). On the basis of the adsorption branches of $N_2$ sorption isotherms, we used the Brunauer−Emmett−Teller (BET) method to calculate the specific surface area ($S_{BET}$) and the Barrett−Joyner−Halenda (BJH) model was used to calculate pore volume (VP), the average pore diameter (DP), and the pore size distribution. FT-IR spectra on pellets of the samples mixed with KBr were recorded on a Nicolet Magna 560 FT-IR spectrometer at a resolution of 4 $cm^{-1}$. Thermal gravity analysis (TG) curves were monitored on a Mettler Toledo 851e apparatus. Photoluminescence (PL) emission spectra were measured on Varian Cary-Eclipse 500 at room temperature under the excitation light at 254 nm.

## 3. RESULTS AND DISCUSSION

The XRD patterns of both pure crystalline $Bi_2TiO_4F_2$ and $C_{60}$ modified crystalline $Bi_2TiO_4F_2$ samples in the wide-angle region are shown in Figure 1. It was found that the as-prepared

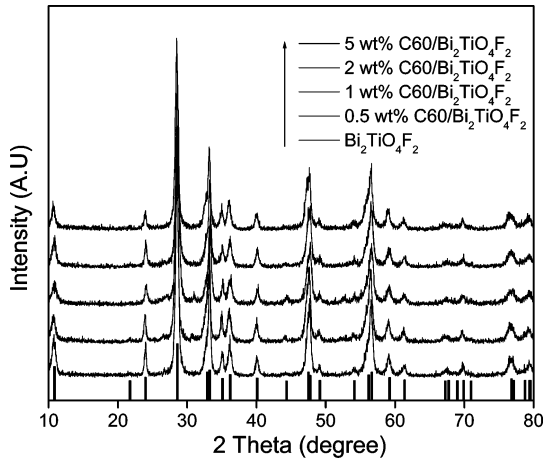


**Figure 1.** XRD patterns of $C_{60}/Bi_2TiO_4F_2$ samples with various $C_{60}$ concentrations.

$Bi_2TiO_4F_2$ samples exhibited intense and sharp diffraction peaks, ascribed to tetragonal $Bi_2TiO_4F_2$ (JCPDS No.33-0219), with lattice constants of $a = b = 3.80$ Å, $c = 16.35$ Å. No other impurities could be observed. We also investigated the crystalline information of the $C_{60}$ modified samples via XRD characterization. Though the modified concentration of $C_{60}$ was increased from 0.5 to 5.0 wt %, the crystalline structure of the tetragonal $Bi_2TiO_4F_2$ phase can still be maintained well, indicating that the combination of $C_{60}$ with the $Bi_2TiO_4F_2$ samples did not alter the crystal structure of the host. It is more interesting that $C_{60}$ phase cannot be detected by XRD even though the mass ratio of $C_{60}$ is as high as 5.0 wt %. As shown in Figure S1 in the Supporting Information, pure C60 exhibits a typical XRD patterns (JCPDS No.44-0558). This maybe attributed to the high dispersion of $C_{60}$ on the surface of $Bi_2TiO_4F_2$ samples.[12]

The morphology of the as-prepared samples was also observed by FESEM. From Fig. 2a-e, it can be seen that both the pure and $C_{60}$ modified samples possessed uniform hierarchical microspheres with $Bi_2TiO_4F_2$ nanosheets assembly. The average size of the $Bi_2TiO_4F_2$ microspheres was slightly enhanced after modifying $C_{60}$. This may be attributed to the aggregation $C_{60}$ located between the $Bi_2TiO_4F_2$ nanosheets. The distribution of $C_{60}$ species was also investigated by the elemental mapping. As shown in Figure 3, Ti-species, Bi-species, O-species, F-species, and C-species elementals were uniformly distributed in the body of the as-obtained $C_{60}/Bi_2TiO_4F_2$ hierarchical microsphere. This clearly displayed that $C_{60}$ were highly dispersed on the surface of the as-prepared samples.

For investigating the effect of $C_{60}$ on the micro/nano structures of $Bi_2TiO_4F_2$, TEM was also utilized to analyze the products on nanoscale. As shown in Figure 4, the pure $Bi_2TiO_4F_2$ samples exhibited spherical structures with lots of nanosheets assembled (Figure 4b). Upon 1.0 wt % C being load, the size of the crystal spheres was slightly increased as shown in Fig. 4c. Such results are consistent with that of the FESEM analysis. Compared to the nanosheets of pure $Bi_2TiO_4F_2$, the surface of the 1.0 wt % $C_{60}/Bi_2TiO_4F_2$ was uniformly covered with lots of $C_{60}$ cluster dots (with an average diameter of 3.0 nm), as demonstrated in Figure 4d. The HRTEM images (Figure 4e) further shows that lots of heterojunctions were formed between the highly crystallized $Bi_2TiO_4F_2$ and $C_{60}$. These results demonstrate that our proposed route could allow the uniformed deposition of $C_{60}$ on the surface of the $Bi_2TiO_4F_2$ nanosheets. As shown in Figure S2 in the Supporting Information, the as-prepared 1.0 wt % $C_{60}/Bi_2TiO_4F_2$ spheres possess a BET surface area of about 25.4 $m^2/g$, similar to that (23.1 $m^2/g$) of the pure $Bi_2TiO_4F_2$ spheres (see Table S1 in the Supporting Information). Furthermore, $C_{60}$ modified samples still own the hierarchical structure with meso- and macropores. Thus, it is reasonable to assume that $C_{60}$ clusters were successfully incorporated in the $Bi_2TiO_4F_2$ samples while keeping its special hierarchical structures.

For further justifying the existence of $C_{60}$ species incorporated in the hybrid system, we applied FTIR to analyze the as-obtained samples. Figure 5a compared the IR spectra of various samples, including $C_{60}$, $Bi_2TiO_4F_2$, and 1.0 wt % $C_{60}/Bi_2TiO_4F_2$. $C_{60}$ molecules present the typical IR peaks at 1183 and 1428 $cm^{-1}$ ascribed to the internal modes of the $C_{60}$.[13] The pure $Bi_2TiO_4F_2$ samples show no $C_{60}$ related peaks. To the case of 1.0 wt % $C_{60}/Bi_2TiO_4$ composites, two typical IR peaks of $C_{60}$ could be well-defined, indicating $C_{60}$ can be trapped by the $Bi_2TiO_4F_2$ nanosheets via the solvothermal route. To prove the strong combination between $C_{60}$ and $Bi_2TiO_4F_2$ nanosheets, we also investigated whether $C_{60}$ can leach from the $C_{60}/Bi_2TiO_4$ hybrid system in toluene solution. As shown in Figure S3 in the Supporting Information, the color of the toluene solution turned to pink upon dispersing the mechanical mixture of 1.0 wt % $C_{60}/Bi_2TiO_4F_2$ (left) in toluene at room temperature for 5 h. However, no color change can be observed to the case of the as-prepared 1.0 wt % $C_{60}/Bi_2TiO_4F_2$ composites at the same conditions. These results clearly show that the loaded $C_{60}$ clusters in the hybrid system nearly cannot be extracted by its excellent solvent (toluene), suggesting an intense interaction

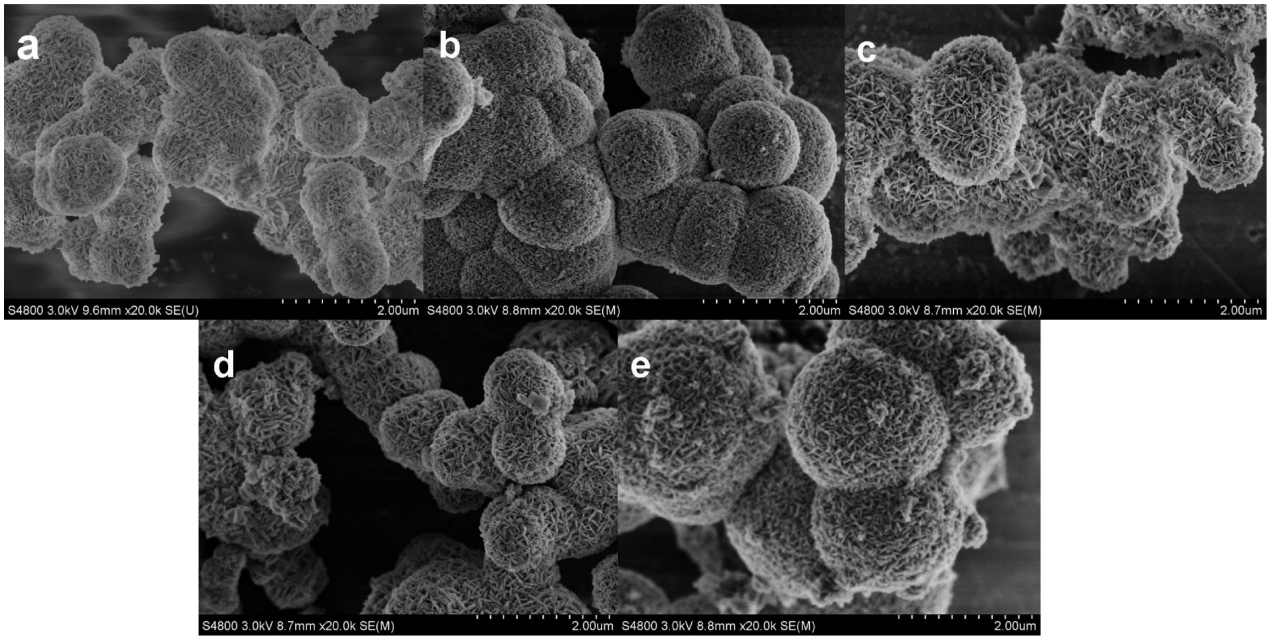


**Figure 2.** FESEM images of $Bi_2TiO_4F_2$ (a), 0.5 wt % $C_{60}/Bi_2TiO_4F_2$ (b) 1.0 wt % $C_{60}/Bi_2TiO_4F_2$ (c), 2.0 wt % $C_{60}/Bi_2TiO_4F_2$ (d), and 5.0 wt % $C_{60}/Bi_2TiO_4F_2$ (e).

formed between $C_{60}$ clusters and $Bi_2TiO_4F_2$. This conclusion can also be supported by the TG-DTA analysis. As shown in Figure 5b, the weight loss rate of the $C_{60}/Bi_2TiO_4F_2$ composites was much slower than that of the mechanical mixture samples, though both of the two samples possessed a similar weight loss percentage (about 6.0 wt %). This indicates that the thermal stability of $C_{60}$ can be greatly enhanced owing to the strong interaction between $C_{60}$ clusters and $Bi_2TiO_4F_2$. Therefore, it can be assumed that the as-prepared $C_{60}/Bi_2TiO_4F_2$ composites will exhibit a good stability in the photocatalytic reaction because $C_{60}$ cannot be dissolved in water (the photocatalytic reaction medium).

As an effective photocatalyst, the light absorption capability (LAC) is very crucial for its photocatalytic performance. Thus, it is highly required to maintain or enhance LAC of the as-prepared $Bi_2TiO_4F_2$ samples even after loading $C_{60}$. Herein, UV−visible diffuse reflectance spectroscopy (DRS) was used to detect the electronic states of the as prepared samples. As shown in Figure 6a, the LAC in both UV and visible-light region was significantly enhanced upon loading $C_{60}$ clusters on the surface of $Bi_2TiO_4F_2$ nanosheets. Besides promoting light absorption, $C_{60}$ was also proved to be able to improve the photocurrent of $Bi_2TiO_4F_2$ samples. As shown in Figure 6b, the $C_{60}$ modified samples could generate significant photocurrents under visible-light irradiation ($\lambda$ > 420 nm). This maybe attributed to the higher light-absorption capability (allowing generating more photo-electrons) and/or higher electron mobility (accelerating the photoelectron transfer). Therefore, all the above results show that the $C_{60}/Bi_2TiO_4F_2$ composites should be an effective photocatalyst system.

The photocatalytic degradation of RhB was utilized as a probe reaction to evaluate the photocatalytic activities of as-prepared sample. Figure 7a shows the decrease of the concentration of RhB in the presence of the as-prepared samples under visible light irradiation ($\lambda$ > 420 nm). Only 65 % RhB can be photo-degraded by pure $Bi_2TiO_4F_2$ under visible light in 120 min. Upon loading $C_{60}$, the photocatalytic performance was greatly enhanced. All the $C_{60}$ modified $Bi_2TiO_4F_2$ samples exhibited much higher photocatalytic activities than pure $Bi_2TiO_4F_2$ under visible-light irradiation. The 1.0 wt % $C_{60}$-modified $Bi_2TiO_4F_2$ sample exhibited the highest activity with an RhB removal rate of 93.0 %. It was also noted that the loaded amount of $C_{60}$ play a great role on the photocatalytic activity of the as-prepared photocatalyst. When the concentration of $C_{60}$ was increased from 0 to 1.0 wt %, the activity of the $C_{60}/Bi_2TiO_4F_2$ composites for degrading RhB was remarkably improved, whereas the photocatalytic activities were decreased upon loading exceeded $C_{60}$ (> 1.0 wt %). As effective photocatalysts, stability is a very important factor for its wide applications in treating pollutants. To evaluate the photochemical stability of the catalyst, we performed the repeated experiments for the photocatalytic decomposition of dyes under the same conditions over as-prepared 1.0 wt %-$C_{60}/Bi_2TiO_4F_2$ composites, and the results are shown in Figure 7b. It revealed that 1.0 wt %-$C_{60}/Bi_2TiO_4F_2$ samples could maintain the high photocatalytic performance for the photocatalytic degradation of RhB even after eight recycles. A slight decrease of the photocatalytic performance was observed. This may be attributed to the loss of the photocatalysts during the recovery process of the photocatalyst via centrifugation. Besides the stability of the photocatalytic performance, we also utilized SEM and TEM to investigate the structural stability of the as-prepared $C_{60}/Bi_2TiO_4F_2$ hybrid system after 8 times of recyclability. As shown in Figure S4 in the Supporting Information, nearly no changes could be observed even after eight recycles, though some fragments could be observed in the TEM images. Such excellent photocatalytic performance (including activity and stability) of $C_{60}/Bi_2TiO_4F_2$ composites may be ascribed to the following advantages: (1) high capability of $C_{60}$ for accelerating electron transfer and enhancing the charge separation efficiency; (2) strong light absorption capability; (3) strong combination between $C_{60}$ and $Bi_2TiO_4F_2$ nanosheets.

As shown in Figure 8, we also compared the photocatalytic removal rates of RhB *via* choosing various functional materials, including pure $C_{60}$, $Bi_2TiO_4F_2$, $C_{60}/Bi_2TiO_4F_2$ composites, and

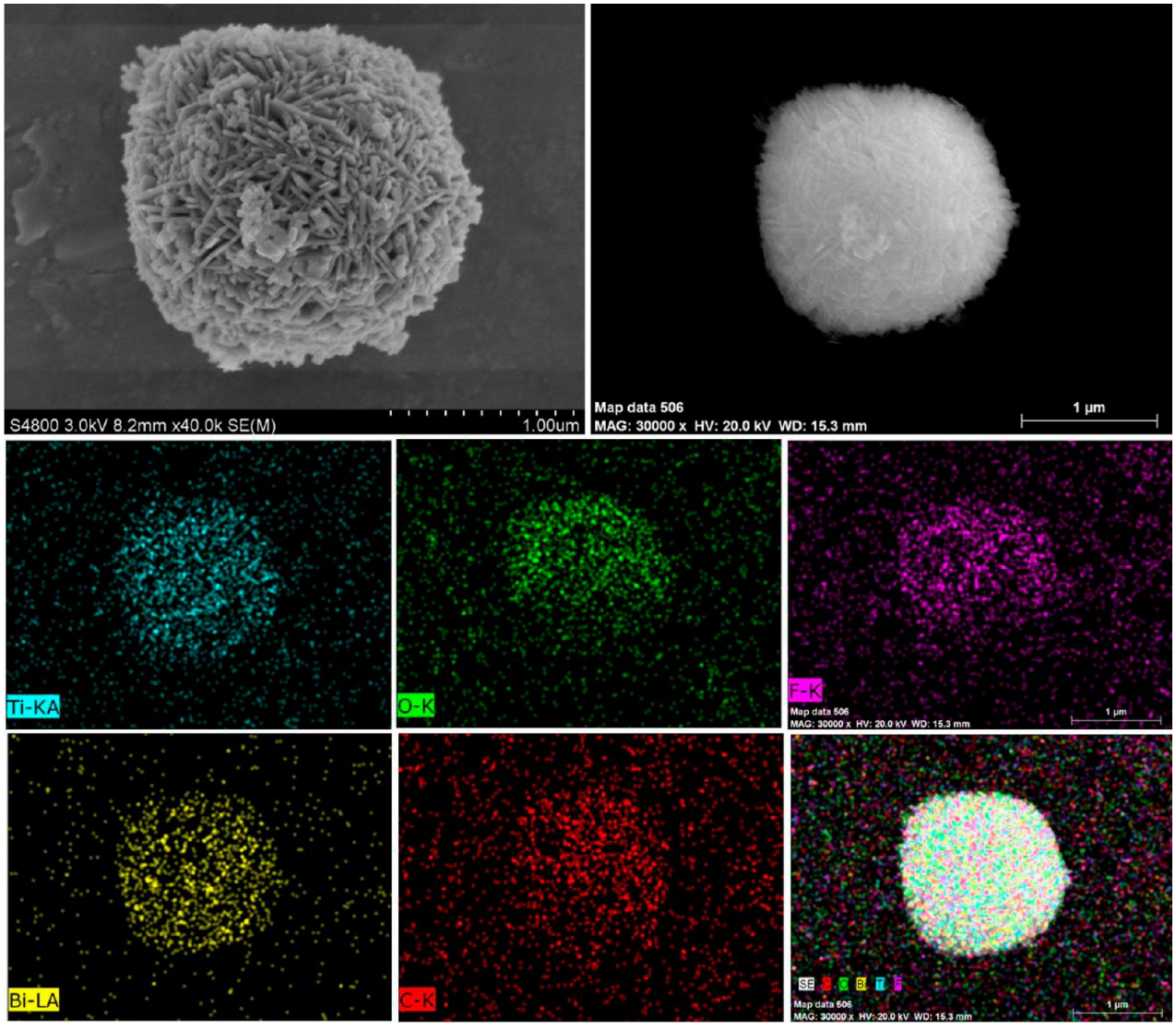


**Figure 3.** FESEM images and FESEM-EDX elemental maping of the 1.0 wt % $C_{60}/Bi_2TiO_4F_2$ spheres.

the mechanical mixture of $Bi_2TiO_4F_2$ and $C_{60}$. The removal rate of RhB can be neglected in the photo-degradation of RhB in the presence of pure $C_{60}$, serving as catalyst. A slightly enhanced photocatalytic removal rate was achieved upon mechanically blending the mixture of $Bi_2TiO_4F_2$ and $C_{60}$ (1.0 wt %). It is interesting that $C_{60}/Bi_2TiO_4F_2$ composites show much higher photocatalytic activity than that of the mechanical mixture of $C_{60}/Bi_2TiO_4F_2$ with the same amount of loaded $C_{60}$. Such greatly enhanced photocatalytic performance of the $C_{60}/Bi_2TiO_4F_2$ composites maybe attributed to the intimate contact between $C_{60}$ and $Bi_2TiO_4F_2$. The formed contacting interface can accelerate the electron transfer between $Bi_2TiO_4F_2$ and $C_{60}$. The difference of photocatalytic performance between $C_{60}/Bi_2TiO_4F_2$ composites and the mechanical mixture of $Bi_2TiO_4F_2$ and $C_{60}$ can also be well illustrated via the photoelectrochemical or photoluminescence (PL) results.

The photocurrent densities of the as-prepared $C_{60}/Bi_2TiO_4F_2$ composites and the mechanical mixture of $Bi_2TiO_4F_2$ and $C_{60}$ were measured in light on-off process with a pulse of 10 s by potentiostatic technique under visible light irradiation ($\lambda$ > 420 nm). All the samples show highly reproducible for numerous on-off cycles. The photocurrent value goes down to zero via turning off the light, and the photocurrent can come back to the original value as soon as the light is turned on again (Figure 9a). It should be noted that the as-prepared $C_{60}/Bi_2TiO_4F_2$ composites exhibit a much higher photocurrent density generation of ca. 27 $\mu A/cm^2$, which is greatly enhanced compared with that of the mechanical mixture sample (with a value of ca. 17 $\mu A/cm^2$). The electrochemical impedance spectroscopy (EIS) results (Figure 9b) shows that the arc radius on the EIS Nynquist plot of $C_{60}/Bi_2TiO_4F_2$ composites is smaller than that of the mechanical mixture sample. This suggests that the former owns a more effective separation of photo-generated electron/hole pairs and faster interfacial charge transfer.[14,15] All the above results demonstrate that the $C_{60}/Bi_2TiO_4F_2$ fabricated by hydrothermal route could separate electron/hole pairs more effectively than those prepared by mechanical mixture strategy, owing to the strong combination between $C_{60}$ and $Bi_2TiO_4F_2$ nanosheets.

To clarify the mechanism of the photocatalytic degradation of aqueous RhB in the presence of the as-prepared $C_{60}/Bi_2TiO_4F_2$ composites, we introduced various reactive species scavengers, including sodium oxalate (10 mg), isopropanol (1.0 mL), $AgNO_3$ (10 mg), and nitrogen gas, to the photocatalytic

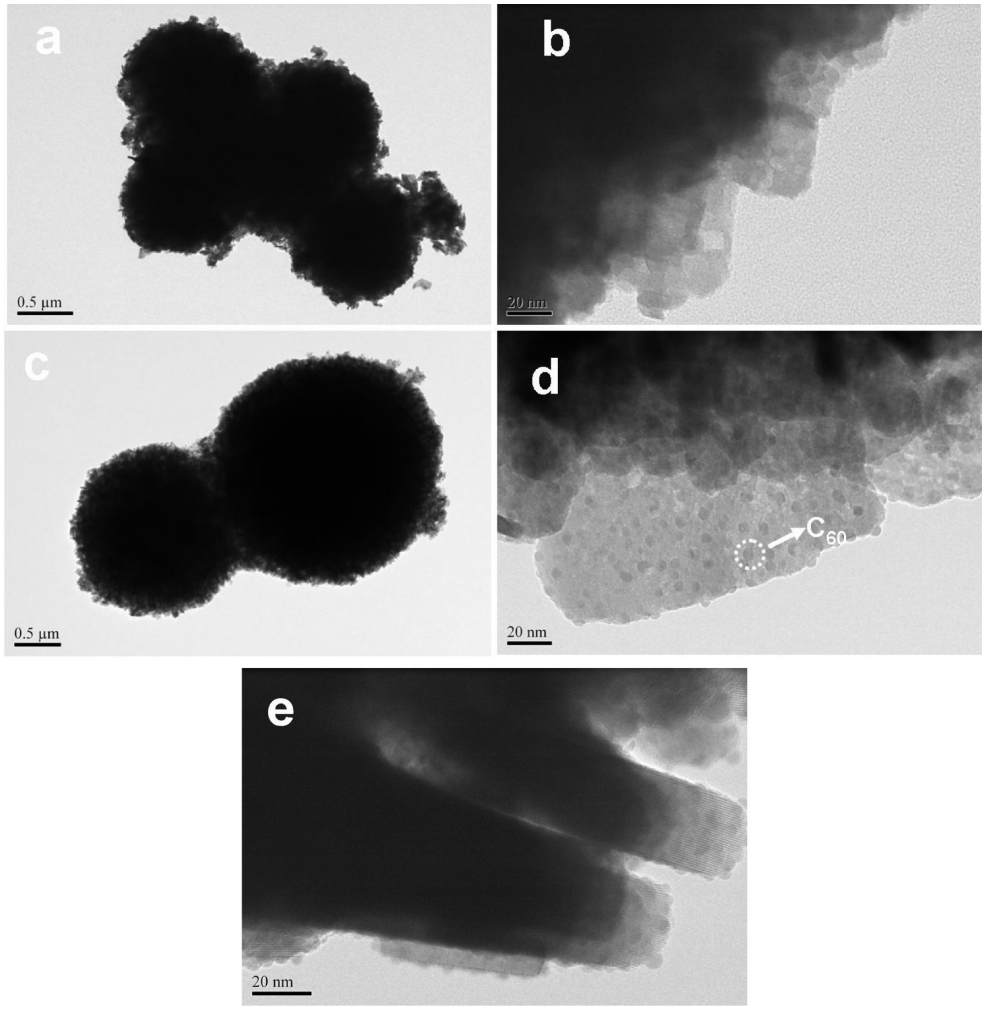


**Figure 4.** TEM images of (a, b) $Bi_2TiO_4F_2$ and (c–e) 1.0 wt % $C_{60}/Bi_2TiO_4F_2$.

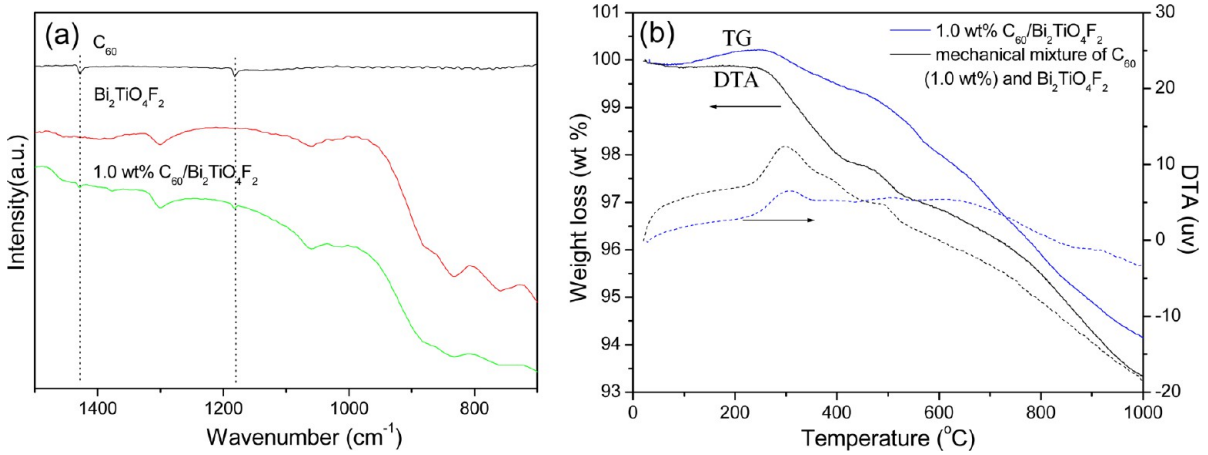


**Figure 5.** (a) FTIR of $C_{60}$, $Bi_2TiO_4F_2$, and 1.0 wt % $C_{60}/Bi_2TiO_4F_2$ composites; (b) TG/DTA curves carried out in air for the mechanical mixture of 1.0 wt % $C_{60}/Bi_2TiO_4F_2$ and the 1.0 wt % $C_{60}/Bi_2TiO_4F_2$ composites.

reaction system for investigating the effect of holes ($hv_{b+}$), hydroxyl radicals (·OH), photo-generated electrons ($e^-$) and oxygen molecules ($\cdot O_2^-$) on the removal efficiency of RhB under visible-light irradiation. As shown in Fig. 10, it was found that a weak decrease of the photocatalytic activity was observed by using isopropanol (IPA) as a hydroxyl radicals (·OH) scavenger. This indicates that the hydroxyl radicals (·OH) are not the key for degrading RhB via photocatalysis. As known, the formation of superoxide anions ($\cdot O_2^-$), an important active radical for photocatalytic reactions, resulted from the reaction between the dissolved oxygen in the reaction system and photo-generated electrons. Upon purging with nitrogen gas, oxygen molecules could be expelled from the present reaction system. This can inhibit the formation of super-oxide anions,

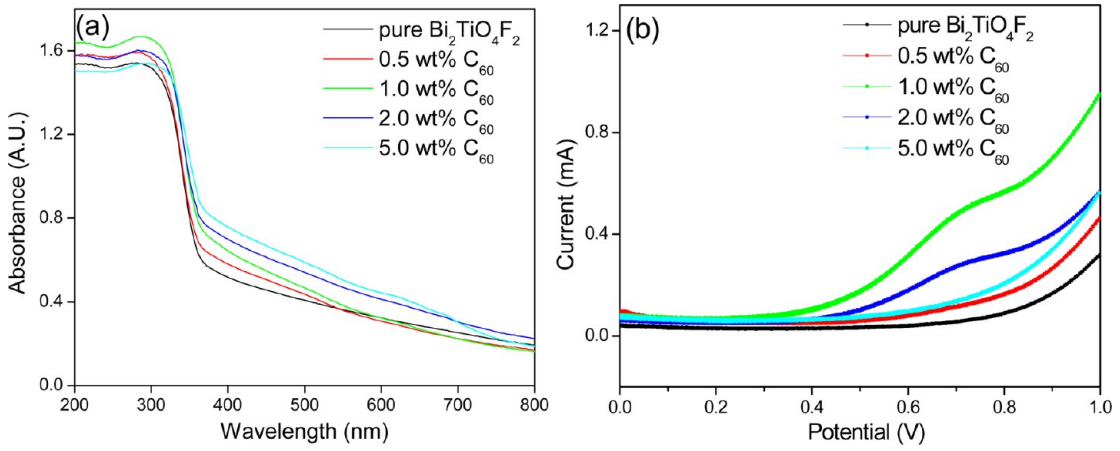


**Figure 6.** (a) UV−vis diffuse reflectance spectra of $C_{60}$ modified $Bi_2TiO_4F_2$ with different $C_{60}$ concentrations; and (b) photocurrent plots of $Bi_2TiO_4F_2$ film and $C_{60}$-modified $Bi_2TiO_4F_2$ films with different $C_{60}$ concentrations as a function of potential under visible light ($\lambda$ > 420 nm).

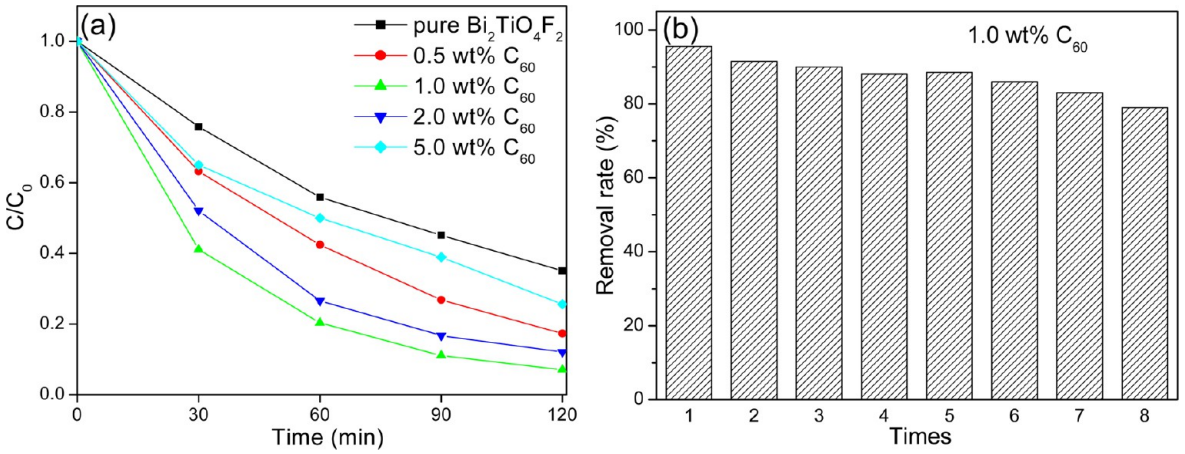


**Figure 7.** (a) Photocatalytic performance of the as-prepared photocatalysts for degrading RhB (20 ppm) as a function of the irradiation time under visible light irradiation ($\lambda$ > 420 nm); (b) recyclability of the photocatalytic degradation of RhB (20 ppm) in the presence of the 1.0 wt % $C_{60}$/ $Bi_2TiO_4F_2$ composites.

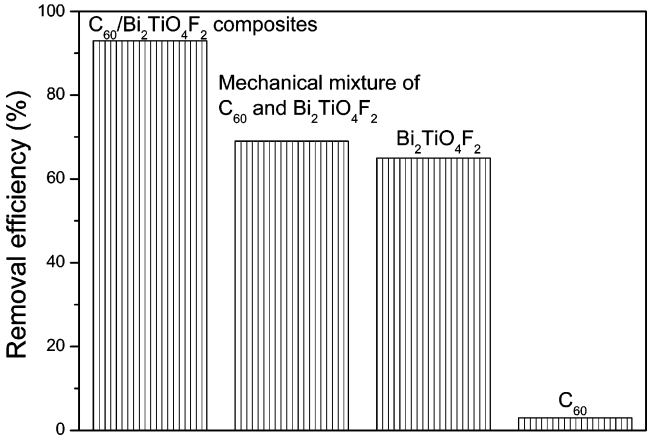


**Figure 8.** Removal efficiency of RhB photo-degradation on $C_{60}$, $Bi_2TiO_4F_2$, mechanical mixture of $C_{60}$ (1.0 wt %) and $Bi_2TiO_4F_2$, and the 1.0 wt % $C_{60}$/ $Bi_2TiO_4F_2$ composites.

resulting in a significant decrease of the removal rate of RhB as shown in Figure 10. Another key to forming the superoxide anions is photo-generated electrons, so $AgNO_3$ was utilized as the electrons scavenger for trapping the photo-generated electrons evolved in the reaction system. It was found that the decrease percentage of the photocatalytic activity was nearly same to that resulted from $N_2$ purging treatment. Such results indicate that $\cdot O_2^-$ played an important role in affecting the photocatalytic performance of the as-formed $C_{60}/Bi_2TiO_4F_2$ composites. It was also noted that a 90.0 % decrease in the photocatalytic activity was attributed to the addition of sodium oxalate ($Na_2C_2O_4$) for trapping photo-generated holes ($h_{vb}^+$). Therefore, it can be concluded that the photo-oxidation mechanism occurring on the surface of $C_{60}/Bi_2TiO_4F_2$ may involve the direct reaction of the organic chemical (dye) with surface $h_{vb}^+$ or a dual mechanism involving both surface $h_{vb}^+$ and $\cdot O_2^-$. It is different from that (photo-generated holes and ·OH radicals played an essential role for the oxidation of RhB) of the pure $Bi_2TiO_4F_2$ reported in our previous work.[5] This may be attributed to fast electrons transfered from $Bi_2TiO_4F_2$ to $C_{60}$ and the formation of high concentrated super-oxide anions in the $C_{60}/Bi_2TiO_4F_2$ composites systems.

To the case of the optimal sample, 1.0 wt % $C_{60}/B_iTiO_4F_2$, the absorptive intensity of RhB at a wavelength of 553 nm gradually decreases and absorption band shifts to shorter wavelengths decrease in absorbance at 509 nm) as shown in Figure S5 in the Supporting INformation. Furthermore, no new absorption bands appear in either the visible or the UV region. This suggests the complete photocatalytic decomposition of

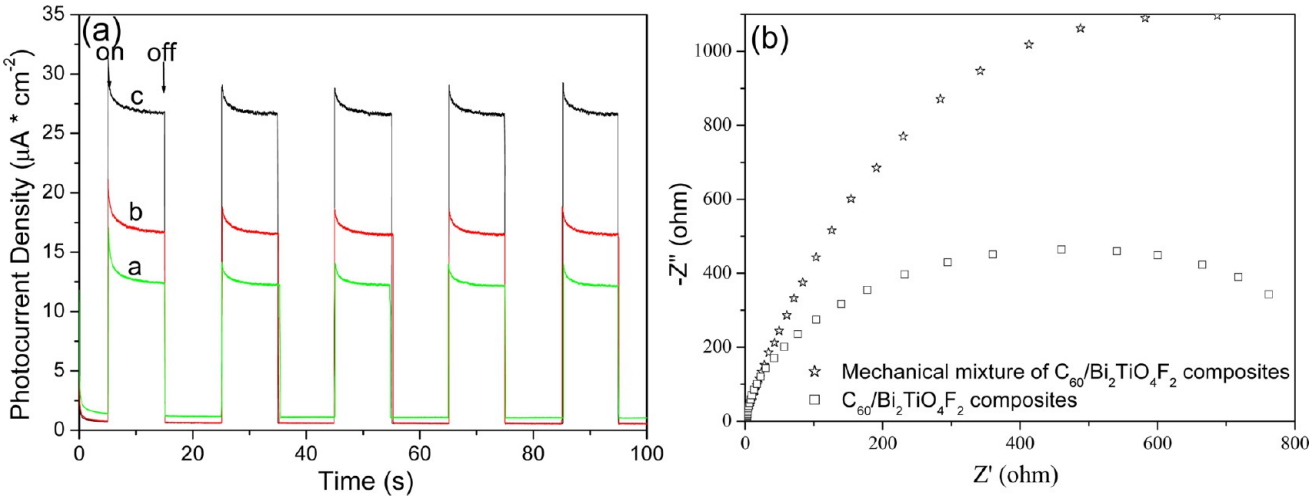


**Figure 9.** (a) Photocurrent responses in light on−off process (0.5 V vs. SCE): (a) pure $Bi_2TiO_4F_2$, (b) mechanical mixture of $C_{60}$ (1.0 wt %) and $Bi_2TiO_4F_2$, and (c) 1.0 wt % $C_{60}/Bi_2TiO_4F_2$ composites. (b) EIS Nynquist plots of the mechanical mixture of $C_{60}$ (1.0 wt %) and $Bi_2TiO_4F_2$ and 1.0 wt % $C_{60}/Bi_2TiO_4F_2$ composites. The bias potential is 0.5 V, under visible-light irradiation ($\lambda$ > 420 nm).

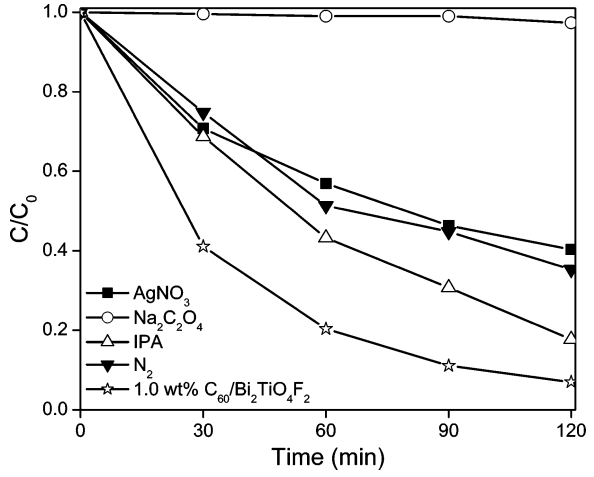


**Figure 10.** Effect of isopropanol (Δ), $Na_2C_2O_4$ (○), $AgNO_3$ (■), and $N_2$ (▼) on the photocatalytic performance of 1.0 wt % $C_{60}/Bi_2TiO_4F_2$ composites for degrading RhB (20 ppm).

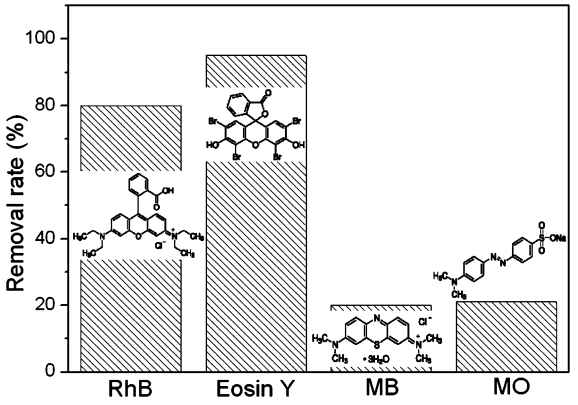


**Figure 11.** Photocatalytic performance of the as-prepared 1.0 wt % $C_{60}/Bi_2TiO_4F_2$ composites for degrading various dyes, including RhB, Eosin Y (EY), methylene blue (MB), and methyl orange, with the concentration of 20 ppm, under visible light irradiation ($\lambda$ > 420 nm) for 1 h.

RhB during the reaction on 1.0 wt % $C_{60}/Bi_2TiO_4F_2$ sample. We have also clarified the mechanism (direct reaction of the organic chemical (dye) with surface $hvb^+$ or a dual mechanism involving both surface $hvb^+$ and $\cdot O_2^-$) of the photocatalytic degradation of aqueous RhB in the presence of the as-prepared $C_{60}/Bi_2TiO_4F_2$ composites in Figure 10. Thus, a possible degradation pathway of RhB was proposed as the following equation

$$hvb^+/\cdot O_2^-. + \text{dye(RhB)} \rightarrow CO_2 + H_2O$$

For investigating the wide usage for environmental remediation of the as-prepared photocatalysts, other dyes, such as Eosin Y, methylene blue, and methyl orange, were also chosen as the target organic molecules to be degraded. As shown in Figure 11, RhB and EY can be significantly decomposed with a high removal rate of 80 and 95%, respectively, under visible-light irradiation for 1 h. At the same condition, the as-obtained $C_{60}/Bi_2TiO_4F_2$ composites can only produce a similar removal rate (about 20 %) after one hour reaction to the case of MB and MO. These results show that large organic molecules were easily to be degraded in the present reaction system. On the contrary, small organic molecules cannot be well decomposed. This may be attributed to its special photocatalytic mechanism based on the surface $h_{vb}^+$ and $\cdot O_2^-$ radicals. Therefore, it is reasonable that the $C_{60}/Bi_2TiO_4F_2$ composites system may exhibit the selectivity for oxidization, instead of complete mineralization. Such a property can be extended to selective catalytic oxidation for achieving useful organic intermediates.

## 4. CONCLUSION

Photocatalyst $C_{60}$-modified $Bi_2TiO_4F_2$ hierarchical microspheres were synthesized using a facile routine solvothermal process. $C_{60}$ clusters (about 3.0 nm) were highly dispersed on the surface of the $Bi_2TiO_4F_2$ crystal nanosheets with the formation of strong heterojunctions between $C_{60}$ and $Bi_2TiO_4F_2$. Such intense interaction enhanced both photogenerated electron transfer rate and charge separation efficiency, and it also improved the light absorption capability and the photocatalytic stability of the $C_{60}/Bi_2TiO_4F_2$ composites. A significant enhanced photocatalytic performance was achieved for degrading RhB and EY under visible light

irradiation with an optimal $C_{60}$ concentration of about 1.0 wt %.

## ■ ASSOCIATED CONTENT

### Supporting Information

Photoelectrochemical measurements; photocatalytic performance testing; Physicochemical properties of the as-prepared $Bi_2TiO_4F_2$ and $C_{60}/Bi_2TiO_4F_2$ samples; XRD patterns of the pure $C_{60}$; BET results of $C_{60}/Bi_2TiO_4F_2$; the photos of the as-prepared samples dispersed in toluene solution; FESEM and TEM images of recycled $C_{60}/Bi_2TiO_4F_2$; UV-visible spectral changes of RhB in an aqueous 1.0 wt % $C_{60}/Bi_2TiO_4F_2$ dispersion as a function of irradiation time under visible light ($\lambda$ > 420 nm) illumination. This material is available free of charge via the Internet at http://pubs.acs.org.

## ■ AUTHOR INFORMATION

### Corresponding Author

*E-mail: Liguisheng@shnu.edu.cn (G.L.); Jianzhu@shnu.edu.cn (J.Z.). Fax: +(86)21-64322272. Tel: +(86)21-64321673.

### Notes

The authors declare no competing financial interest.

## ■ ACKNOWLEDGMENTS

This work was supported by the Program for Professor of Special Appointment (Eastern Scholar) at Shanghai Institutions of Higher Learning, the National Natural Science Foundation of China (21007040, 21237003, and 21261140333), Shanghai Government (11SG42, 11PJ1407500, 10160503200, 11ZR1426300, DXL122), PCSIRT (IRT1269), and by a scheme administrated by Shanghai Normal University (SK201104, DXL122, and S30406).

## ■ REFERENCES

(1) Brown, M. A.; De Vito, S. C. *Crit. Rev. Environ. Sci. Technol.* **1993**, *23*, 249−324.
(2) Long, Y. Z.; Lu, Y.; Huang, Y.; Peng, Y. C.; Lu, Y. J.; Kang, S. Z.; Mu, J. *J. Phys. Chem. C* **2009**, *113*, 13899−13905.
(3) Hoffmann, M. R.; Martin, S. T.; Choi, W.; Bahnemann, D. W. *Chem. Rev.* **1995**, *95*, 69−96.
(4) Yu, J. C.; Ho, W.; Yu, J.; Yip, H.; Wong, P. K.; Zhao, J. *Environ. Sci. Technol.* **2005**, *39*, 1175−1179.
(5) Jiang, B.; Zhang, P.; Zhang, Y.; Wu, L.; Li, H. X.; Zhang, D. Q.; Li, G. S. *Nanoscale* **2012**, *4* (2), 455−460.
(6) Lee, J.; Fortner, J. D.; Hughes, J. B.; Kim, J. H. *Environ. Sci. Technol.* **2007**, *41*, 2529−2535.
(7) Chen, C.; Zhao, W.; Lei, P.; Zhao, J.; Serpone, N. *Chem.—Eur. J.* **2004**, *10*, 1956−1965.
(8) Kalinowski, J.; Giro, G.; Camaioni, N.; Fattori, V.; Di Marco, P. *Synth. Met.* **1996**, *77*, 181−188.
(9) Nierengarten, J. F.; Gu, T.; Aernouts, T.; Geens, W.; Poortmans, J.; Hadziioannou, G.; Tsamouras, D. *Appl. Phys. A* **2004**, *79*, 47−49.
(10) Zhu, S. B.; Xu, T. G.; Fu, H. B.; Zhao, J. C.; Zhu, Y. F. *Environ. Sci. Technol.* **2007**, *41*, 6234−6239.
(11) Dong, G. F.; Zheng, H. Y.; Duan, L.; Wang, L. D.; Qiu, Y. *Adv. Mater.* **2009**, *21*, 2501−2054.
(12) Zhang, J.; Yu, J. G.; Zhang, Y. M.; Li, Q.; Gong, J. R. *Nano Lett.* **2011**, *11*, 4774−4779.
(13) Fu, H. B.; Xu, T. G.; Zhu, S. B.; Zhu, Y. F. *Environ. Sci. Technol.* **2008**, *42*, 8064−8069.
(14) Zhang, Y.; Zhang, P.; Huo, Y. N.; Zhang, D. Q.; Li, G. S.; Li, H. X. *Appl. Catal., B* **2012**, *115*, 236−244.
(15) Hao, Z.; Ruilong, Z.; Jincai, Z.; Yongfa, Z. *Environ. Sci. Technol.* **2008**, *42*, 3803−3807.